ACS APPLIED MATERIALS & INTERFACES

Research Article

www.acsami.org

Aerosol Jet Printed p- and n-type Electrolyte-Gated Transistors with a Variety of Electrode Materials: Exploring Practical Routes to Printed Electronics

Kihyon Hong,[†] Se Hyun Kim,[†,‡] Ankit Mahajan,[†] and C. Daniel Frisbie*[,†]

[†]Department of Chemical Engineering & Materials Science, University of Minnesota, 421 Washington Avenue SE, Minneapolis, Minnesota 55455, United States

[‡]Department of Advanced Organic Materials Engineering, Yeungnam University, 280 Daehak-ro, Gyeongsan 712-749, Korea

Supporting Information

ABSTRACT: Printing electrically functional liquid inks is a promising approach for achieving low-cost, large-area, additive manufacturing of flexible electronic circuits. To print thin-film transistors, a basic building block of thin-film electronics, it is important to have several options for printable electrode materials that exhibit high conductivity, high stability, and low-cost. Here we report completely aerosol jet printed (AJP) p- and n-type electrolyte-gated transistors (EGTs) using a variety of different electrode materials including highly conductive metal nanoparticles (Ag), conducting polymers (polystyrenesulfonate doped poly(3,4-ethylendedioxythiophene, PEDOT:PSS), transparent conducting oxides (indium tin oxide), and carbon-based materials (reduced graphene oxide). Using these source-drain electrode materials and a PEDOT:PSS/ion gel gate stack, we demonstrated all-printed p- and n-type EGTs in combination with poly(3-hexythiophene) and ZnO semiconductors. All transistor components (including electrodes, semiconductors, and gate insulators) were printed by AJP. Both kinds of devices showed typical p- and n-type transistor characteristics, and exhibited both low-threshold voltages (<2 V) and high hole and electron mobilities. Our assessment suggests Ag electrodes may be the best option in terms of overall performance for both types of EGTs.

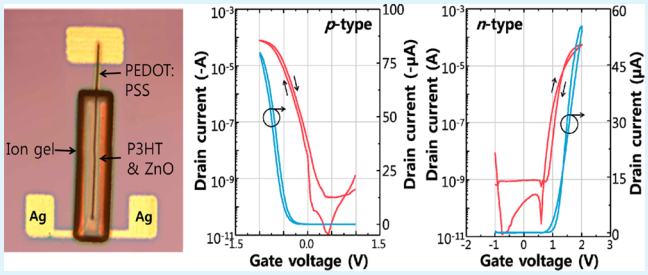

KEYWORDS: *electrolyte-gated transistors, electrode materials, aerosol jet printing, ion-gel gate insulator*

1. INTRODUCTION

Recently, electrolyte-gated transistors (EGTs) have emerged as promising devices for printed electronics.[1−3] One of the principal advantages of EGTs is the enormous capacitance (>1 μF/cm^2) of the gate insulator stack, which facilities very low voltage (<2 V) operation.[4,5] Other advantages include the low contact resistances and high carrier mobilities for EGTs based on polymer semiconductors, as well as the possibility of a "side-gate" architecture, which aids fabrication.[4,6−8] Also EGTs are favorable with regard to printing process compatibility. Because the capacitance (but not switching speed) of the electrolyte is independent of its thickness, we can conveniently realize low-voltage EGTs by printing, which has been a challenging hurdle for flexible electronics.[9]

A potential complication for EGTs is the compatibility of the electrolyte with the source, drain, and gate electrode materials. For example, a possible problem is electrochemical instability for metals under bias in contact with the electrolyte.[9] Gold (Au) is a leading electrode material due to its excellent conductivity (4×10^7 S/m) and chemical stability.[3,10,11] Also, p-type EGTs with Au electrodes have low contact resistance, which leads to good effective hole mobilities (~1 cm^2 V^{-1} s^{-1}) and low threshold voltages (V_{th}).[7,12] However, Au can induce large electron injection barriers in n-type EGTs due to its relatively high work function (~5.3 eV). In addition, it is expensive.[13] Conducting polymers such as polystyrenesulfonate doped poly(3,4-ethylendedioxythiophene) (PEDOT:PSS) can be good alternatives to Au. Printed p-type EGTs with PEDOT:PSS source-drain electrodes also perform reasonably well.[9,14] However, PEDOT has a substantially lower conductivity than conventional metals, and this leads to parasitic resistance effects in devices employing PEDOT contacts. Thus, development of high-quality alternative electrode materials for EGTs remains an important challenge. As far as we are aware, no investigation to date has systematically examined the performance of all-printed EGTs with various kinds of electrode materials. There are of course previous reports of all inkjet-printed thin-film transistors (TFTs) using different materials.[15,16]

In this paper, we systematically examined the performance of all-printed p- and n-type EGTs with various kinds of source-drain electrode materials including metal nanoparticles (Ag),

Received: July 1, 2014
Accepted: October 17, 2014
Published: October 17, 2014

   dx.doi.org/10.1021/am504171u | ACS Appl. Mater. Interfaces 2014, 6, 18704−18711

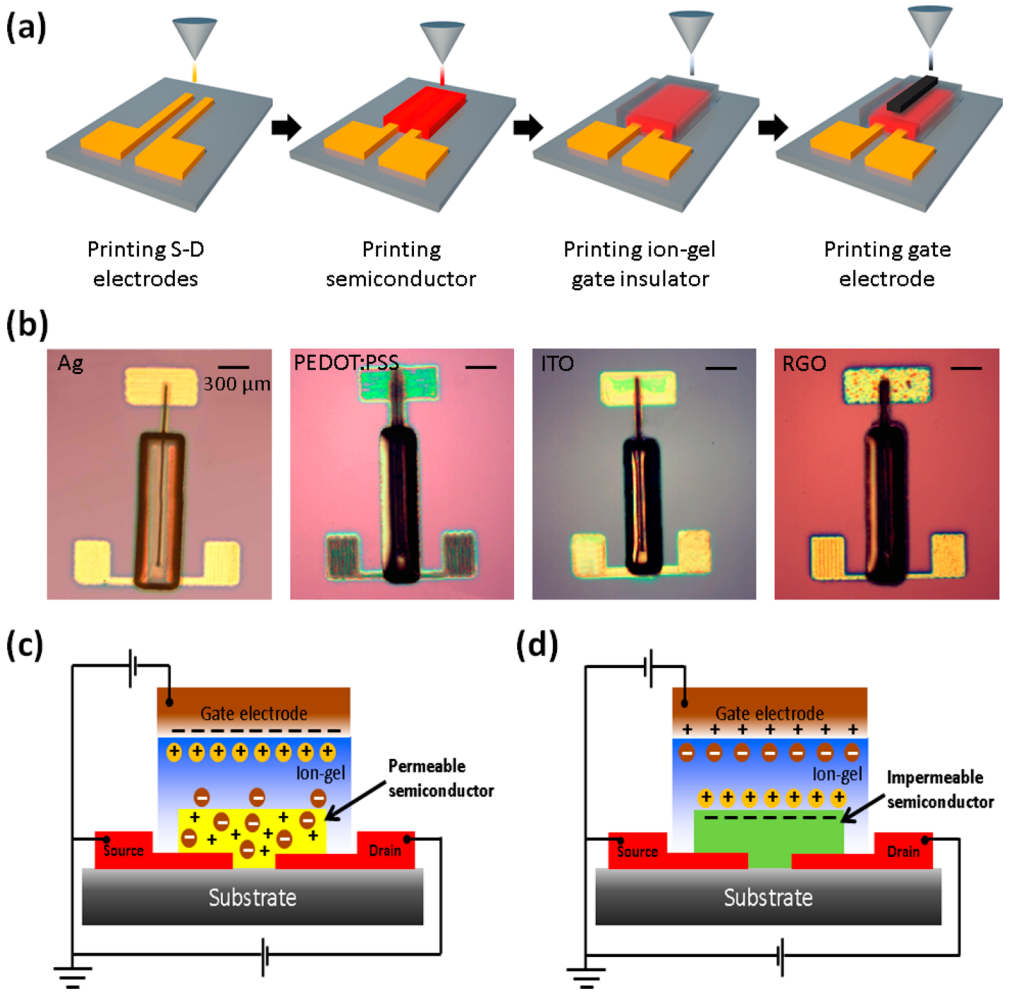

Figure 1. (a) Additive fabrication of EGTs by aerosol jet printing on SiO_2/Si substrates. A top gate (PEDOT:PSS), bottom contact EGT architecture was used in this study with W/L = 1000 μm/50 μm. (b) Optical microscope images of printed EGTs with different kinds of S-D electrode materials: Ag, PEDOT:PSS, ITO, and annealed RGO. (c, d) Cross sections and operation mechanisms of a p-type EGT with permeable polymer semiconductor and an n-type EGT with impermeable metal oxide semiconductor.

the conducting polymer PEDOT:PSS, transparent conducting oxides (i.e., indium tin oxide (ITO)), and reduced graphene oxide (RGO). A commercial aerosol jet printer was used for printing of all EGT components (i.e., the source-drain electrodes, gate insulator, semiconductor, and gate electrodes). Aerosol jet printing (AJP) employs a dense aerosol with droplets between 1 and 5 μm in diameter. The aerosol stream is focused to a collimated beam by surrounding it with a second, sheath gas stream. Printed lines can be as narrow as 10 μm. Thus, AJP is a versatile method for patterning a wide range of electronically functional liquid inks including precursor inks, nanoparticle suspensions, diluted electronic pastes, and biological materials.[17] As a printable electrolyte gate insulator, we employed ion gels consisting of an ionic liquid and triblock copolymer, as reported previously.[1,4,5] Sheet resistances of the printed source-drain (S-D) electrodes were evaluated as a function of annealing temperature. Work functions of each material were examined using ultraviolet photoelectron spectroscopy (UPS). Both p-type and n-type EGTs with these S-D materials showed high charge carrier mobilities and low threshold voltages, V_{th} (<2 V). On the basis of these results, we discuss the correlation between the physical properties of the printed S-D electrodes and overall printed EGT performance.

2. EXPERIMENTAL SECTION

Aerosol Jet Printing. All printing was done using the AJ 200 benchtop aerosol jet printer (Optomec, Inc.). The stage was heated to 60 °C for all printing steps to aid in solvent evaporation. The carrier gas (N_2) and sheath gas (N_2) flow rates, as well as nozzle diameter, varied as specified below. Stage speed was generally 1 mm/s. Printing was done in air.

Printing Ag Electrodes. The Ag ink contained 40 wt % Ag nanoparticles, with particle diameters <20 nm (Ag40X, UT Dots Inc.), dispersed in a solvent mixture of xylene and terpineol (9:1 by volume). The prepared ink was printed on SiO_2/Si substrates. A 150 μm diameter nozzle was used for printing, and the flow rate of N_2 carrier gas was 20 sccm. A sheath gas flow rate of 50 sccm was used to focus the printed Ag stream. The printed samples were sintered at 200 °C in air for 30 min in a box furnace.

Printing PEDOT:PSS Electrodes. The PEDOT:PSS ink was prepared by mixing 10% by volume ethylene glycol with 90% Heraeus PH500 aqueous PEDOT:PSS ink. The carrier and sheath gas flow rates were 20 and 40 sccm, respectively. A 150 μm diameter nozzle was used for printing, and substrate temperature was maintained at 60 °C.

Printing ITO Electrodes. ITO ink was prepared according to the conventional sol–gel procedure.[18] $In(NO_3)_3{\cdot}2H_2O$ and $SnCl_2$ (9:1 w/w), used as starting materials, were dissolved in a mixture (9:1 v/v) of ethanol and acetylacetone (0.08 g/mL). The solution was stirred at room temperature for 3 h. A 150 μm diameter nozzle was used for

dx.doi.org/10.1021/am504171u | ACS Appl. Mater. Interfaces 2014, 6, 18704–18711

printing, and the carrier gas/sheath gas flow ratio was 15 sccm/25 sccm. The printed ITO samples were heat-treated at 500 °C for 1 h under ambient air.

Printing RGO Electrodes. Graphene oxide (GO) was produced by a modified Hummers method.[18] To obtain dispersions for AJP, the dried GO powder (1 mg) was added to deionized water (2 mL) contained within a vial, which was then sonicated for 12 h. The dispersion was printed on a substrate with a 150 μm diameter nozzle. The flow rate of carrier gas and sheath gas were 15 and 30 sccm, respectively. The stage temperature was maintained at 60 °C during printing. To reduce the as-printed GO film, samples were placed in a clean glass Petri dish inside a larger glass Petri dish that contained 1 mL of hydrazine hydrate solution. ***Caution!*** *Hydrazine is hazardous in case of skin contact or inhalation*. The larger dish was covered with a glass lid, sealed with Parafilm tape, and placed over a hot plate at 100 °C for 12 h. After the chemical reduction, the dish was opened, and the sample was rinsed with purified water. To improve the conductivity of RGO, printed samples were annealed in vacuum (10^{-3} Torr) at 200 °C for 2 h.

Device Fabrication. SiO_2/Si wafers with AJ printed source-drain electrodes (Ag, PEDOT:PSS, ITO, and annealed RGO) were used as substrates. The channel lengths were 50 μm, and the channel widths were 1000 μm. To form a p-type semiconductor layer, poly(3-hexylthiophene) (P3HT) was printed on the substrate. The P3HT ink was prepared by dissolving the polymer (1 mg/mL) in a solvent mixture of chloroform and terpineol (9:1 by weight). A 150 μm diameter nozzle was used for printing, and the carrier gas/sheath gas flow ratio was 15 sccm/25 sccm. For printing n-type semiconductor, ZnO ink was used. The ZnO ink was prepared by dissolving 2 mg of ZnO (Sigma-Aldrich 99.999%) into 1 mL of ammonium hydroxide (aq) (Alfa Aesar, 99.9%). A 250 μm diameter nozzle was used for printing. The flow rate of carrier gas and sheath gas were 12 and 25 sccm, respectively. The resulting ZnO film was annealed at 300 °C for 1 h in ambient air. A layer of ion-gel ink including the polystyrene−poly(methyl methacrylate)−polystyrene (PS−PMMA−PS) triblock copolymer and 1-ethyl-3-methylimidazolium bis-(trifluoromethylsulfonyl) imide ([EMIM][TFSI]) ionic liquid in ethyl acetate at a 1:9:90 ratio (w/w/w) was printed on the semiconductor films as a gate insulator. To form the gate electrode, PEDOT:PSS was printed over the channel region. All printing steps were carried out in air with stage temperature maintained at 60 °C to enhance ink drying. Transistor current−voltage characteristics were measured using Keithley 2400 and 236 source measuring units. The devices, which were not intentionally encapsulated, were measured in ambient nitrogen to minimize unwanted effects of H_2O and O_2.

3. RESULTS AND DISCUSSION

The additive printing process for EGTs is illustrated in Figure 1a and is described in detail in the Experimental Section. All EGT components including S-D electrodes, organic/inorganic semiconductors, ion-gel gate insulators, and gate electrodes were printed on SiO_2/Si substrates using the AJP method (Figure 1b).[3] Four kinds of electrode materials, namely, Ag nanoparticle, PEDOT:PSS, ITO, and RGO were printed on the substrate as S-D electrodes (W/L = 1000 μm/50 μm). After printing S-D electrodes, P3HT and ZnO were printed on the channel regions as p-type and n-type semiconductor materials, respectively. As a printable gate insulator material, we employed large-capacitance (>1 μFcm^{-2}) ion-gel electrolyte. It is reported that the ion gel shows capacitance value of ~10 μF/cm^2 at low (<10 Hz) frequency. Finally, the conducting polymer, PEDOT:PSS, was printed on the ion-gel layer as a top gate electrode.

For the p-type EGTs based on P3HT, ions from the ion gel can penetrate into the channel layer. The P3HT channel is three-dimensional due to this ion penetration, resulting simultaneously in enormous drain current levels, low operation voltage (<1 V), and high hole carrier mobility (~1 cm^2 V^{-1} s^{-1}) in the device (Figure 1c).[1,4,19] In the case of EGTs with n-type ZnO semiconductor, ions cannot penetrate the dense ZnO, and instead electrical double layers (EDLs) are formed at the gate/ion gel and ion gel/semiconductor interfaces under applied gate bias (Figure 1d). The channel for the ZnO EGTs is two-dimensional, but because the EDL capacitance is very large, of order 1 μF/cm^2, the ZnO EGTs also exhibit low voltage operation (<2 V) and high ON-current levels.[4,20,21] Another advantage of employing the ion gel as a printable gate insulator is its process compatibility. We previously reported that the low-frequency capacitance of the ion gel is independent of its thickness in the range of 1−10 μm.[9] This means that relatively thick layers of ion gel can be coated on the semiconductor layer. Because thickness control in the sub-100 nm regime is a challenging hurdle for printing technology, using ion-gel gate insulator in which the thickness is not critical can clearly be a processing advantage.

Figure 2a shows the optical microscope image of aerosol jet printed Ag electrodes produced using a nanoparticle ink. The thickness and minimum width of printed lines were 500 nm and 50 μm, respectively. The Ag nanoparticles were protected by an organic ligand to prevent premature coalescence in solution.[22] Thus, as-printed Ag nanoparticles film were electrically insulating, and a thermal sintering process was required to achieve high conductivity. Considerable particle sintering and connections between nanoparticles were observed in the atomic force microscope (AFM) image of a sintered Ag (200 °C) sample (see Supporting Information, Figure S1). The surface roughness of the annealed Ag film was 280 nm. The sheet resistances (R_S) of printed Ag nanoparticles on SiO_2/Si substrates were evaluated as a function of sintering temperatures as shown in Figure 2b. The R_S of the films dropped rapidly to 4.6 ohm/sq, that is, several orders of magnitude upon sintering at 200 °C for 30 min. Sintering at higher temperatures did not produce significant further increases in conductivity. Importantly, 200 °C is a low enough sintering temperature to be compatible with Kapton (polyimide) substrates. Other recently developed Ag inks can be sintered at temperatures as low as 100 °C, which opens up opportunities for processing on polyester substrates.[23]

Using the printed Ag patterns, we fabricated all-printed p-type and n-type EGTs (W/L = 1000 μm/50 μm) with P3HT and ZnO semiconductor materials, respectively. Figure 2d,e shows the transfer and output curves of P3HT EGTs. The devices showed typical p-type transistor characteristics, and we observed good saturation behavior in the output curves. The field effect mobility and threshold voltage were calculated to be 1.7 cm^2 V^{-1} s^{-1} and −0.40 V, respectively, using the standard linear regime field effect transistor equation (see Table 1). The threshold voltage was determined by linear extrapolation of the I_D−V_G plot (V_D = 0.1 V). The output curve exhibited the desirable linear and saturation regimes with a clear gate-voltage dependence. The electrical characteristics of n-type EGTs with ZnO channels are displayed in Figure 2f,g. The field effect mobility and ON/OFF ratio calculated from the transfer curve in the linear regime were 1.5 cm^2 V^{-1} s^{-1} and 10^4, respectively.

The conducting polymer PEDOT:PSS has received much attention as an electrode material for printed electronics because of its printability, low fabrication cost, and mechanical flexibility.[9,24] Using AJP, we printed PEDOT:PSS patterns having thickness of 750 nm and minimum line width of 40 μm in a single pass of the print nozzle (Figure 3a). Unlike printed

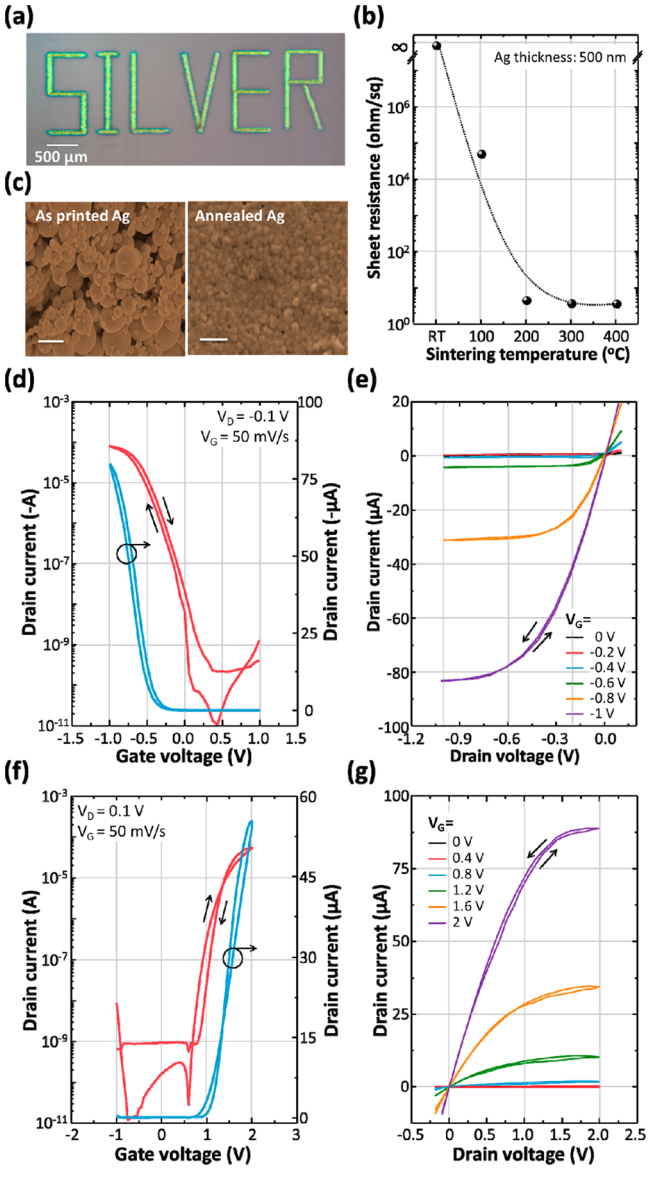

Figure 2. Ag electrodes. (a) Optical microscope image of a printed Ag pattern on SiO_2/Si. The thickness and minimum width of the printed lines are ~500 nm and 50 μm, respectively. (b) Sheet resistance of printed Ag films as a function of sintering temperature. Each sample was sintered for 1 h in air. The dashed line is a guide to the eyes. (c) Scanning electron microscopy images of as-printed (left) and sintered (200 °C, right) Ag samples. Scalebar: 1 μm. (d, e) Quasi-static (voltage sweep rate: 50 mV/s) transfer and output characteristics of printed p-type EGTs with P3HT semiconductor and Ag S-D electrodes. (f, g) Quasi-static electrical properties of n-type EGTs with ZnO semiconductor and Ag S-D electrodes. The printed Ag electrodes were sintered at 200 °C.

Ag, it is known that annealing can degrade the conductivity of PEDOT. However, to investigate the suitability of the printed PEDOT:PSS electrodes for n-type EGTs with ZnO channels, which require thermal annealing, we examined the change of R_S as a function of annealing temperature (Figure 3b). The R_S values of as-printed PEDOT samples were measured to be 960 Ω/sq, and the values slightly increased upon annealing up to 200 °C for 30 min. At 300 °C, however, the R_S increased drastically to ~22 kΩ/sq. Annealing at 500 °C resulted in electrically insulating films. It has been reported that the large

Table 1. Threshold Voltages and Effective Mobilities of Printed p-type (P3HT) and n-type (ZnO) EGTs with Various Electrode Materials

	P3HT-EGTs		ZnO-EGTs	
	V_{th} (V)	mobility (p) (cm^2 V^{-1} s^{-1})	V_{th} (V)	mobility (n) (cm^2 V^{-1} s^{-1})
Ag	−0.30	1.73	0.90	1.48
PEDOT:PSS	−0.35	1.63	1.00	0.16
ITO	−0.25	1.08	1.05	0.81
RGO	−0.35	0.41	0.30	0.59

increases in R_S upon annealing above 200 °C originate from over oxidation and degradation of the polymer (Figure 3c).[25,26]

The electrical characteristics of p-type and n-type EGTs with PEDOT:PSS S-D electrodes were measured and are displayed in Figure 3d–g. The transfer curve of the p-type EGT showed an OFF-current level of 10^{-9} A and an ON/OFF current ratio of ~10^5. The field effect hole mobility was 1.6 cm^2 V^{-1} s^{-1}. The drain current of the output curve increased linearly at low drain voltage, indicating that hole injection from the PEDOT:PSS source electrode to the P3HT layer is efficient. For n-type EGTs, the field effect mobility, V_{th}, and ON/OFF ratio were 0.2 cm^2 V^{-1} s^{-1}, 1.0 V, and 10^4, respectively.

One advantage of using transparent conducting oxides as electrode materials is that they can be applicable to driving circuits for display pixels or transparent electronics.[27] Figure 4a shows an optical microscope image of aerosol jet printed ITO patterns. The thickness and minimum width of printed patterns were 500 nm and 50 μm, respectively. Figure 4b shows the variation of R_S of printed ITO films as a function of annealing temperature. The samples were annealed for 1 h at each temperature in air. The as-printed ITO sample exhibited electrically insulating behavior. However, during the annealing process, there was a strong reduction in R_S to 2250 Ω/sq at 500 °C. Increases in conductivity for ITO are known to be correlated with crystallinity; specifically, the Sn dopants become more active in crystalline ITO. To investigate the crystallinity, X-ray diffraction (XRD) was performed on as-printed and annealed (500 °C) samples (Figure 4c). The resulting diffraction spectra indicated that the as-printed ITO is amorphous. After annealing, the film showed evidence of conversion from an amorphous to polycrystalline cubic bixbyite In_2O_3 structure having preferred orientation of (222), consistent with the idea that the conductivity increase with annealing arises from a change in microstructure.[28−30]

The electrical properties of P3HT EGTs with ITO electrodes were characterized by measuring the transfer and output curves, as shown in Figure 4d,e. The obtained ON/OFF current ratio was 10^4, and V_{th} was found to be −0.25 V. The field effect mobility was estimated to be 1.1 cm^2 V^{-1} s^{-1}. For n-type EGTs, V_{th} was 1.05 V, and field effect mobility was 0.8 cm^2 V^{-1} s^{-1}. Both p-type and n-type EGTs exhibited very small hysteresis at a quasi-static gate voltage sweep rate of 50 mV/s, which is common for EGTs.[31,32] Hysteresis in EGTs is a function of both the ion-gel thickness and the nature of the semiconductor (e.g., whether ions penetrate the semiconductor or not). Optimization of the dynamic performance of the EGTs is the focus of further studies.[4,9]

Because of its unique electrical, chemical, and mechanical properties, graphene has been considered an attractive electrode material for transistors, sensors, and optoelectronic devices.[33,34] Because graphene oxide (GO) can be dispersed

dx.doi.org/10.1021/am504171u | ACS Appl. Mater. Interfaces 2014, 6, 18704−18711

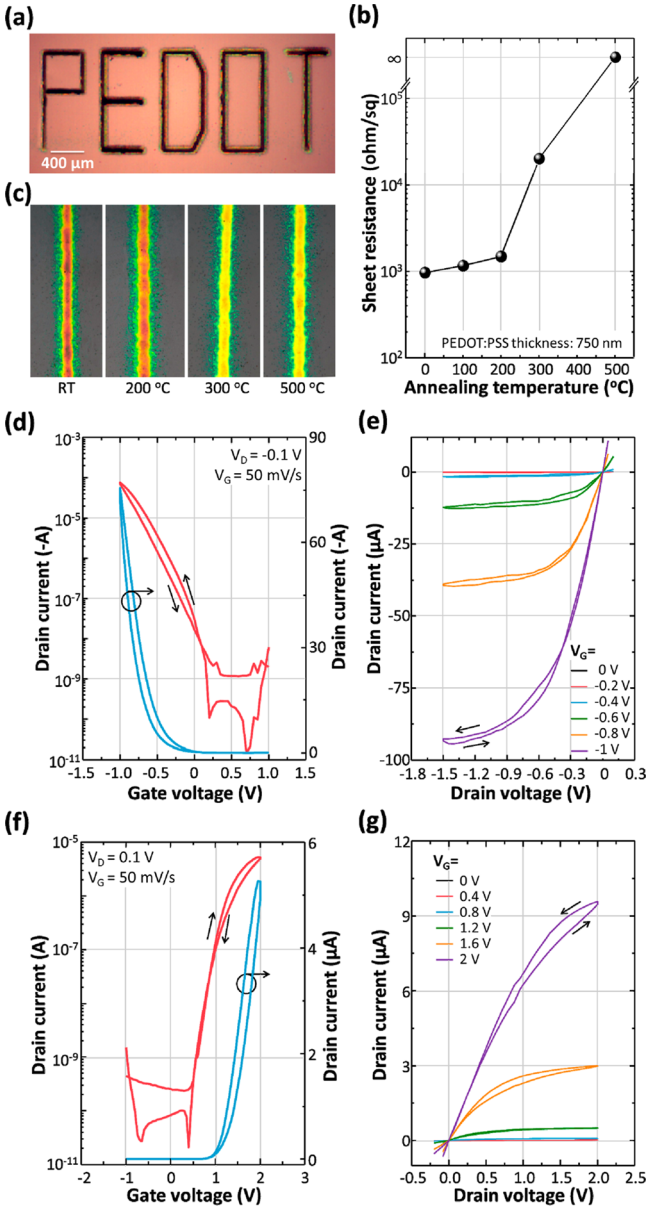

Figure 3. PEDOT electrodes. (a) Optical microscope image of a printed PEDOT:PSS pattern on SiO_2/Si. The thickness and minimum width of the printed lines is 750 nm and 40 μm, respectively. (b) Sheet resistance and (c) optical microscope images of printed PEDOT:PSS films as a function of annealing temperatures. The samples were annealed for 1 h in air. (d, e) Quasi-static (voltage sweep rate: 50 mV/s) transfer and output characteristics of printed p-type EGTs with PEDOT:PSS S-D electrodes. Effective field effect hole mobility was calculated to be 1.6 $cm^2 V^{-1} s^{-1}$. (f, g) Quasi-static electrical properties of n-type EGTs with PEDOT:PSS electrodes. To prevent the degradation of PEDOT:PSS, ZnO film was annealed at 200 °C for 1 h. The device showed effective electron mobility value of 0.2 $cm^2 V^{-1} s^{-1}$.

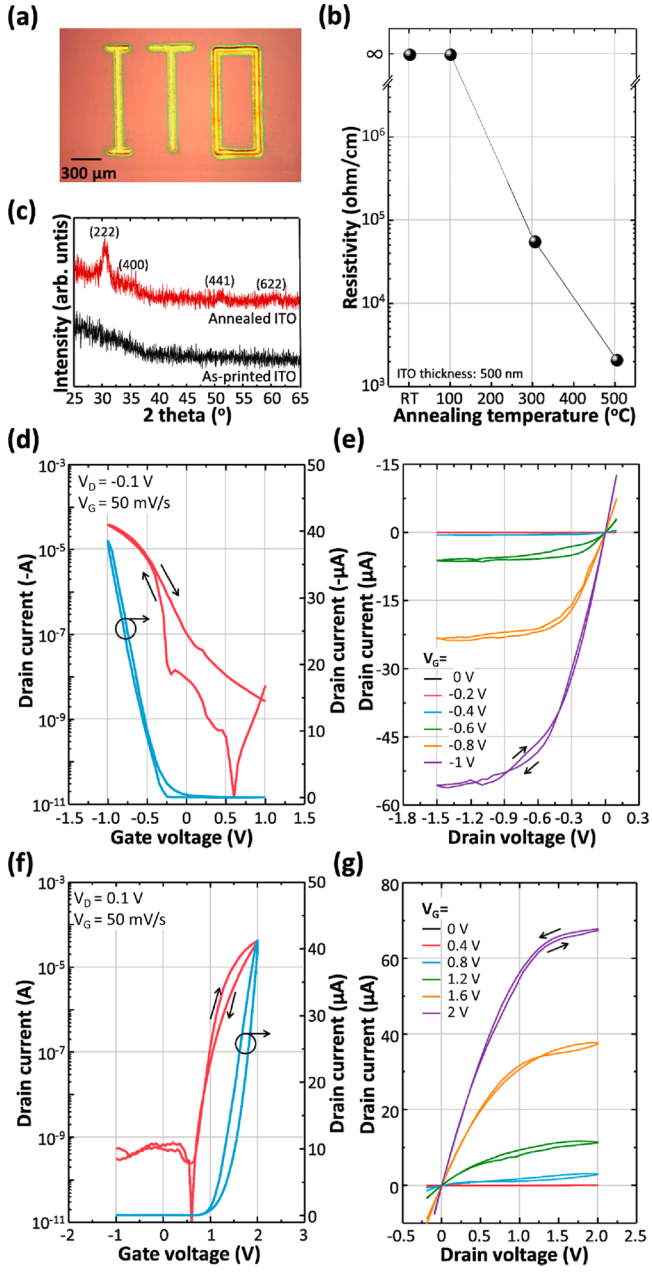

Figure 4. ITO electrodes. (a) Optical microscope image of a printed ITO pattern on SiO_2/Si. The thickness and minimum width of the printed lines is 500 nm and 50 μm, respectively. (b) Sheet resistance of ITO samples as a function of annealing temperatures. The sample annealed at 500 °C showed the lowest R_S value of 2250 Ω/sq. (c) XRD spectra of ITO films on SiO_2/Si substrate as a function of annealing temperatures. (d, e) Quasi-static (voltage sweep rate: 50 mV/s) transfer and output characteristics of printed p-type EGTs with ITO S-D electrodes. Effective hole mobility was 1.1 $cm^2 V^{-1} s^{-1}$. (f, g) Quasi-static electrical properties of n-type EGTs with ITO electrodes. The effective electron mobility and V_{th} were 0.8 $cm^2 V^{-1} s^{-1}$ and 1.05 V, respectively. The annealing temperature of ITO was 500 °C.

easily in water, we prepared water-based GO ink (0.5 mg/mL) and printed it using AJP (Figure 5a). The printed GO patterns had a thickness of 300 nm and minimum line width of 40 μm. The AFM image of annealed RGO sample showed that the film is composed of dense GO droplets between 1 and 5 μm in diameter (See Supporting Information, Figure S1). Figure 5b shows the changes of R_S of printed GO film with different reduction processes. By chemical reduction with hydrazine solution, the insulating GO changed to conductive reduced graphene oxide (RGO, R_S = 20,000 Ω/sq). When this RGO sample was annealed at 200 °C in vacuum for 2 h, the R_S of the sample was further decreased to 6500 Ω/sq (annealed RGO). The change of chemical composition of three kinds of samples, namely, as-printed GO, chemical reduced RGO, and annealed RGO were investigated by X-ray photoemission spectroscopy

dx.doi.org/10.1021/am504171u | ACS Appl. Mater. Interfaces 2014, 6, 18704−18711

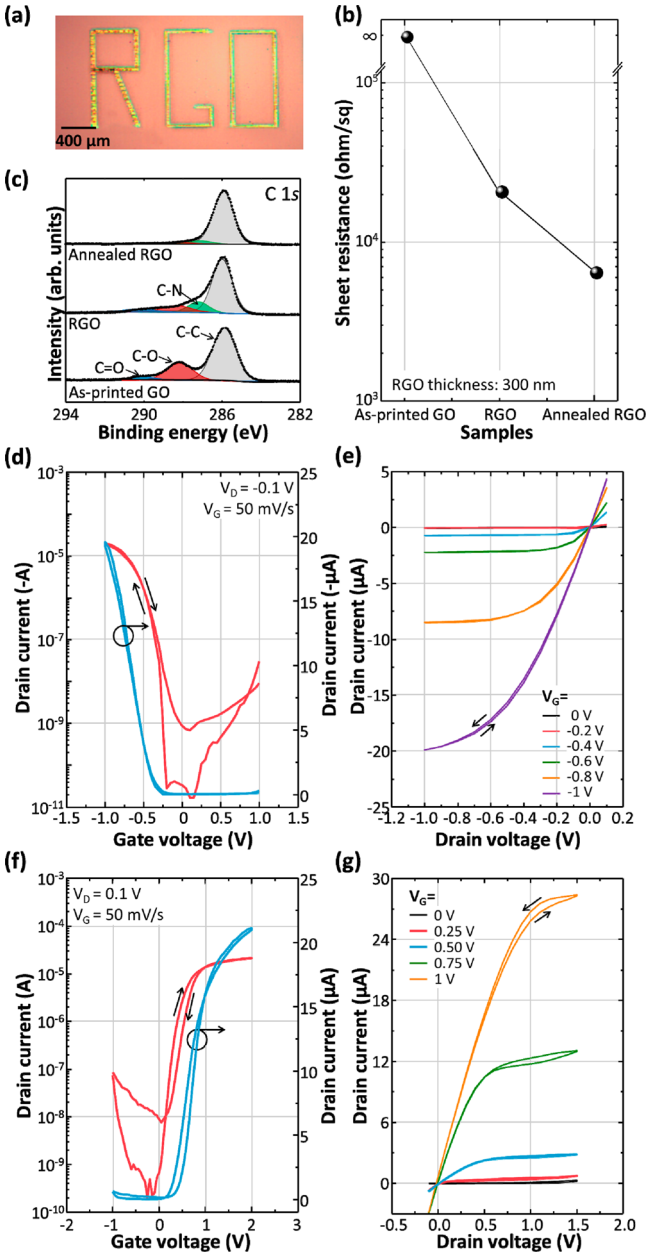

Figure 5. RGO electrodes. (a) Optical microscope image of a printed RGO pattern on SiO_2/Si. The thickness and minimum width of the printed lines is 300 nm and 40 μm, respectively. (b) Changes of sheet resistance of as-printed GO, RGO, and annealed RGO samples. Annealed RGO sample showed the lowest R_S value of 6500 Ω/sq. (c) XPS C 1s spectra of three kinds of GO samples. During the reduction and annealing process, the intensity ratio of I_{C-O}/I_{C-C} decreased from 0.34 to 0.05. (d, e) Quasi-static (voltage sweep rate = 50 mV/s) transfer and output characteristics of printed p-type EGTs with annealed RGO electrodes. (f, g) Quasi-static electrical properties of n-type EGTs with annealed RGO electrodes. p-type and n-type EGTs showed effective mobilities of 0.4 and 0.6 $cm^2\ V^{-1}\ s^{-1}$, respectively.

(XPS). The C 1s peaks were deconvoluted into three chemically shifted components, sp^2 carbon (C−C, 285.8 eV), C−O bond (288.1 eV), and carbonyl group (C═O, 290.09 eV).[35] The as-printed sample showed a relatively large amount of the C−O and C═O component, and the intensity ratio of I_{C-O}/I_{C-C} was 0.34. After chemical reduction (RGO), a new C−N bond appeared, and the peak intensities for C−O and C═O peaks were smaller (I_{C-O}/I_{C-C} = 0.15) than those in as-printed GO.[36,37] The annealed RGO sample showed smallest value of I_{C-O}/I_{C-C} = 0.05. This analysis revealed that the amount of carbon not bound to oxygen (i.e., the C−C peak) followed the same trend as the film conductivity, indicating chemical reduction and thermal annealing processes can effectively reduce the as-printed GO to a more conductive state. The Raman spectra of the three different samples display two prominent peaks at 1340 and 1600 cm^{-1}, which correspond to the well-documented D (absent in perfect graphite) and G (in-plane bond-stretching motion of the sp^2-bonded carbon atom) bands, respectively (see Supporting Information, Figure S2). The reduced and annealed sample exhibited a slight increase in the D/G ratio. This observation suggests that, while most of the oxygenated groups were removed, the RGO still had a high quantity of structural defects.[38]

Figure 5d,e shows the transfer and output characteristics of a printed p-type EGT with annealed RGO electrodes (W/L = 1000 μm/50 μm). The field effect mobility, ON/OFF ratio, V_{th}, and subthreshold swing were 0.4 $cm^2\ V^{-1}\ s^{-1}$, 10^4, −0.35 V, and 95 mV/decade, respectively. For n-type EGTs with ZnO layer, the device showed mobility of 0.6 $cm^{-1}\ V^{-1}\ s^{-1}$, ON/OFF ratio of 10^3, and V_{th} of 0.3 V (Figure 5f,g).

The evolution of V_{th} with respect to the S-D work functions of p-type and n-type EGTs with various electrode materials are plotted in Figure 6a. The work functions of the electrode materials were measured by UPS (see Supporting Information, Figure S3). For p-type EGTs with P3HT, the V_{th} of devices (−0.3 V) were independent of the electrode work functions (Table 1). In the case of n-type EGTs with ZnO, however, V_{th} increased when the work function of electrodes increased. These results can be explained by charge injection efficiency at the electrode/semiconductor interface. It is known that the ionization potential energy of P3HT is ∼5.1 eV.[39] Using the vacuum-level alignment rule for simplicity and the work functions of printed electrode materials (4.70−5.35 eV), the hole injection barriers at the electrodes/P3HT interfaces are in the range of 0−0.4 eV (Figure 6c). Thus, the V_{th} values of p-type EGTs changed less sensitively to the changes in work function of electrode materials. For ZnO, the lower edge of the conduction band (E_C) is located at ∼4.2 eV.[40] Thus, the energy level differences between the Fermi level (E_F) of the various electrodes and the E_C of ZnO can be estimated to be 0.5−1.15 eV (Figure 6d). Because of these large electron injection barriers and wide variation, the V_{th} of n-type EGTs showed large dependence on work functions of electrode materials.

Figure 6b shows the field-effect mobilties of p-type and n-type EGTs as a function of measured R_S of the electrode materials. As the R_S decreased, the effective field-effect mobilities increased; EGTs with Ag electrodes showing the highest mobilities both for holes and electrons. The relatively small mobility of n-type EGTs with PEDOT:PSS electrodes was caused by the lower annealing temperature employed for the ZnO layer (200 °C) than that of other devices (300 °C), to avoid degradation of PEDOT:PSS electrode (Figure 3b,c).[41] In terms of effective carrier mobilities (which are influenced by contact resistance), it appears that Ag electrodes yield the best performance for both p- and n-type EGTs. In terms of threshold voltage, however, RGO electrodes are advantageous for n-type EGTs. For practical applications, however, the off-current level (I_D at V_G = 0 V) would need to be decreased.

dx.doi.org/10.1021/am504171u | ACS Appl. Mater. Interfaces 2014, 6, 18704−18711

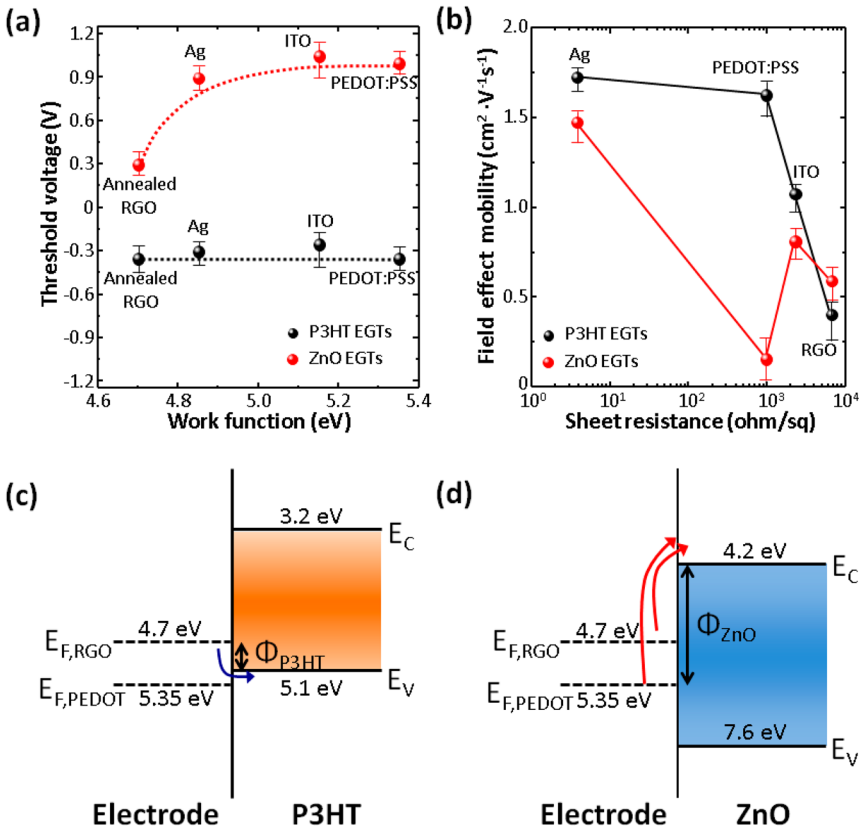

Figure 6. (a) Plot of the correlation between the work function (WF) of electrodes and the threshold voltages of p-type and n-type EGTs. (b) Evolution of the effective mobilities of both p-type and n-type EGTs with respect to the sheet resistance of electrode materials. (c, d) Schematic energy band diagrams in the case of electrode/p-type semiconductor (P3HT) and electrode/n-type semiconductor (ZnO) interfaces. E_F and Φ indicate the Fermi energy level and charge injection barrier, respectively. (The Mott–Schottky limit, i.e., vacuum level alignment, is assumed for simplicity.) The WFs of RGO and PEDOT:PSS are shown because they have the lowest (4.7 eV) and highest (5.35 eV) values, respectively.

4. CONCLUSIONS

We have demonstrated all-printed p-type and n-type EGTs with various electrode materials. All EGT components were fabricated by aerosol jet printing. Ag nanoparticles, PEDOT:PSS, ITO, and annealed RGO were adopted as printable electrode materials. The sheet resistance of the printed electrode materials were in the range of 3–6500 Ω/sq. To realize low-voltage device operation, a printable high-capacitance ion-gel gate insulator was employed. The P3HT and ZnO EGTs showed typical p-type and n-type transistor characteristics, respectively, and exhibited low threshold voltage (<2 V) and high hole and electron effective mobilities up to 1.7 $cm^2\ V^{-1}\ s^{-1}$ and 1.5 $cm^2\ V^{-1}\ s^{-1}$, respectively. For p-type EGTs, the V_{th} was independent of electrode work functions ($V_{th} \approx -0.3$ V). In the case of n-type EGTs, V_{th} increased from 0.3 to 1.05 V corresponding to the increase of electrode work function. The characterization of printed electrode materials can provide guidance for the identification of new materials that are suitable for use in printed EGTs, as well as in the design of circuit structures. Our ongoing work aims to integrate P3HT and ZnO EGTs into high-speed complementary circuits on flexible substrates.

■ ASSOCIATED CONTENT

Supporting Information

Atomic force microscope (AFM) height images of the annealed Ag and RGO samples. Raman spectra of as-printed GO, RGO, and annealed RGO samples. Secondary cutoff spectra of printed S-D electrode materials using a UPS He I (21.2 eV) line. This material is available free of charge via the Internet at http://pubs.acs.org.

■ AUTHOR INFORMATION

Corresponding Author

*E-mail: frisbie@umn.edu.

Notes

The authors declare no competing financial interest.

■ ACKNOWLEDGMENTS

C.D.F. acknowledges the Air Force Office of Scientific Research STTR program (FA8650-13-C-5172) for financial support of this work.

■ REFERENCES

(1) Kim, S. H.; Hong, K.; Lee, K. H.; Frisbie, C. D. Performance and Stability of Aerosol-Jet-Printed Electrolyte-Gated Transistors Based on Poly(3-Hexylthiophene). *ACS Appl. Mater. Interfaces* **2013**, *5*, 6580–6585.

(2) Dasgupta, S.; Stoesser, G.; Schweikert, N.; Hahn, R.; Dehm, S.; Kruk, R.; Hahn, H. Printed and Electrochemically Gated, High-Mobility, Inorganic Oxide Nanoparticle Fets and Their Suitability for High-Frequency Applications. *Adv. Funct. Mater.* **2012**, *22*, 4909–4919.

(3) Cho, J. H.; Lee, J.; Xia, Y.; Kim, B.; He, Y.; Renn, M. J.; Lodge, T. P.; Frisbie, C. D. Printable Ion-Gel Gate Dielectrics for Low-Voltage Polymer Thin-Film Transistors on Plastic. *Nat. Mater.* **2008**, *7*, 900–906.

(4) Kim, S. H.; Hong, K.; Xie, W.; Lee, K. H.; Zhang, S.; Lodge, T. P.; Frisbie, C. D. Electrolyte-Gated Transistors for Organic and Printed Electronics. *Adv. Mater.* **2013**, *25*, 1822−1846.
(5) Ha, M.; Seo, J. W.; Prabhumirashi, P. L.; Zhang, W.; Geier, M. L.; Renn, M. J.; Kim, C. H.; Hersam, M. C.; Frisbie, C. D. Aerosol Jet Printed, Low Voltage, Electrolyte Gated Carbon Nanotube Ring Oscillators with Sub-5 Mus Stage Delays. *Nano Lett.* **2013**, *13*, 954−960.
(6) Lee, K. H.; Kang, M. S.; Zhang, S.; Gu, Y.; Lodge, T. P.; Frisbie, C. D. "Cut and Stick" Rubbery Ion Gels as High Capacitance Gate Dielectrics. *Adv. Mater.* **2012**, *24*, 4457−4462.
(7) Braga, D.; Ha, M.; Xie, W.; Frisbie, C. D. Ultralow Contact Resistance in Electrolyte-Gated Organic Thin Film Transistors. *Appl. Phys. Lett.* **2010**, *97*, 193311.
(8) Pu, J.; Yomogida, Y.; Liu, K. K.; Li, L. J.; Iwasa, Y.; Takenobu, T. Highly Flexible Mos2 Thin-Film Transistors with Ion Gel Dielectrics. *Nano Lett.* **2012**, *12*, 4013−4017.
(9) Xia, Y.; Zhang, W.; Ha, M.; Cho, J. H.; Renn, M. J.; Kim, C. H.; Frisbie, C. D. Printed Sub-2 V Gel-Electrolyte-Gated Polymer Transistors and Circuits. *Adv. Funct. Mater.* **2010**, *20*, 587−594.
(10) Fabiano, S.; Braun, S.; Fahlman, M.; Crispin, X.; Berggren, M. Effect of Gate Electrode Work-Function on Source Charge Injection in Electrolyte-Gated Organic Field-Effect Transistors. *Adv. Funct. Mater.* **2014**, *24*, 695−700.
(11) Kim, B. J.; Jang, H.; Lee, S. K.; Hong, B. H.; Ahn, J. H.; Cho, J. H. High-Performance Flexible Graphene Field Effect Transistors with Ion Gel Gate Dielectrics. *Nano Lett.* **2010**, *10*, 3464−3466.
(12) Dhoot, A. S.; Yuen, J. D.; Heeney, M.; McCulloch, I.; Moses, D.; Heeger, A. J. Beyond the Metal-Insulator Transition in Polymer Electrolyte Gated Polymer Field-Effect Transistors. *Proc. Natl. Acad. Sci. U. S. A.* **2006**, *103*, 11834−11837.
(13) Pang, S.; Tsao, H. N.; Feng, X.; Müllen, K. Patterned Graphene Electrodes from Solution-Processed Graphite Oxide Films for Organic Field-Effect Transistors. *Adv. Mater.* **2009**, *21*, 3488−3491.
(14) Zirkl, M.; Sawatdee, A.; Helbig, U.; Krause, M.; Scheipl, G.; Kraker, E.; Ersman, P. A.; Nilsson, D.; Platt, D.; Bodo, P.; Bauer, S.; Domann, G.; Stadlober, B. An All-Printed Ferroelectric Active Matrix Sensor Network Based on Only Five Functional Materials Forming a Touchless Control Interface. *Adv. Mater.* **2011**, *23*, 2069−2074.
(15) Tseng, H.-Y.; Subramanian, V. All Inkjet-Printed, Fully Self-Aligned Transistors for Low-Cost Circuit Applications. *Org. Electron.* **2011**, *12*, 249−256.
(16) Basiricò, L.; Cosseddu, P.; Fraboni, B.; Bonfiglio, A. Inkjet Printing of Transparent, Flexible, Organic Transistors. *Thin Solid Films* **2011**, *520*, 1291−1294.
(17) Li, S.; Park, J. G.; Wang, S.; Liang, R.; Zhang, C.; Wang, B. Working Mechanisms of Strain Sensors Utilizing Aligned Carbon Nanotube Network and Aerosol Jet Printed Electrodes. *Carbon* **2014**, *73*, 303−309.
(18) Soon Choi, K.; Park, Y.; Kwon, K.-C.; Kim, J.; Keun Kim, C.; Kim, S. Y.; Hong, K.; Lee, J.-L. Reduced Graphite Oxide-Indium Tin Oxide Hybrid Materials for Use as a Transparent Electrode. *J. Electrochem. Soc.* **2011**, *158*, J231.
(19) Kergoat, L.; Herlogsson, L.; Braga, D.; Piro, B.; Pham, M. C.; Crispin, X.; Berggren, M.; Horowitz, G. A Water-Gate Organic Field-Effect Transistor. *Adv. Mater.* **2010**, *22*, 2565−2569.
(20) Hong, K.; Kim, S. H.; Lee, K. H.; Frisbie, C. D. Printed, Sub-2v Zno Electrolyte Gated Transistors and Inverters on Plastic. *Adv. Mater.* **2013**, *25*, 3413−3418.
(21) Lee, K. H.; Zhang, S.; Lodge, T. P.; Frisbie, C. D. Electrical Impedance of Spin-Coatable Ion Gel Films. *J. Phys. Chem. B* **2011**, *115*, 3315−3321.
(22) Kim, D.; Jeong, S.; Shin, H.; Xia, Y.; Moon, J. Heterogeneous Interfacial Properties of Ink-Jet-Printed Silver Nanoparticulate Electrode and Organic Semiconductor. *Adv. Mater.* **2008**, 3084−3089.
(23) Walker, S. B.; Lewis, J. A. Reactive Silver Inks for Patterning High-Conductivity Features at Mild Temperatures. *J. Am. Chem. Soc.* **2012**, *134*, 1419−1421.
(24) Luzio, A.; Musumeci, C.; Newman, C. R.; Facchetti, A.; Marks, T. J.; Pignataro, B. Enhanced Thin-Film Transistor Performance by Combining 13,6-N-Sulfinylacetamidopentacene with Printed Pedot:Pss Electrodes. *Chem. Mater.* **2011**, *23*, 1061−1069.
(25) Huang, J.; Miller, P. F.; Wilson, J. S.; Mello, A. J.; Mello, J. C.; Bradley, D. D. C. Investigation of the Effect of Doping and Post-Deposition Treatments on the Conductivity, Morphology, and Work Function of Poly(3,4-Ethylenedioxythiophene)/Poly(Styrene Sulfonate) Films. *Adv. Funct. Mater.* **2005**, *15*, 290.
(26) Kim, Y.; Ballantyne, A.; Nelson, J.; Bradley, D. Effects of Thickness and Thermal Annealing of the Pedot:Pss Layer on the Performance of Polymer Solar Cells. *Org. Electron.* **2009**, *10*, 205−209.
(27) Hong, S.-J.; Kim, Y.-H.; Han, J.-I. Development of Ultrafine Indium Tin Oxide (Ito) Nanoparticle for Ink-Jet Printing by Low-Temperature Synthetic Method. *IEEE Trans. Nanotechnol.* **2008**, *7*, 172.
(28) Kim, Y. J.; Jin, S. B.; Kim, S. I.; Choi, Y. S.; Choi, I. S.; Han, J. G. Effect of Oxygen Flow Rate on Ito Thin Films Deposited by Facing Targets Sputtering. *Thin Solid Films* **2010**, *518*, 6241−6244.
(29) Morikawa, H.; Fujita, M. Crystallization and Electrical Property Change on the Annealing of Amorphous Indium-Oxide and Indium-Tin-Oxide Thin Films. *Thin Solid Films* **2000**, *359*, 61.
(30) Ting, C.-C.; Cheng, W.-L.; Lin, G.-C. Structural and Opto-Electrical Properties of the Tin-Doped Indium Oxide Thin Films Fabricated by the Wet Chemical Method with Different Indium Starting Materials. *Thin Solid Films* **2011**, *519*, 4286−4292.
(31) Yuan, H.; Shimotani, H.; Tsukazaki, A.; Ohtomo, A.; Kawasaki, M.; Iwasa, Y. High-Density Carrier Accumulation in Zno Field-Effect Transistors Gated by Electric Double Layers of Ionic Liquids. *Adv. Funct. Mater.* **2009**, *19*, 1046−1053.
(32) Thiemann, S.; Sachnov, S.; Porscha, S.; Wasserscheid, P.; Zaumseil, J. Ionic Liquids for Electrolyte-Gating of Zno Field-Effect Transistors. *J. Phys. Chem. C* **2012**, *116*, 13536−13544.
(33) Pang, S.; Hernandez, Y.; Feng, X.; Mullen, K. Graphene as Transparent Electrode Material for Organic Electronics. *Adv. Mater.* **2011**, *23*, 2779−2795.
(34) Yu, W. J.; Chae, S. H.; Lee, S. Y.; Duong, D. L.; Lee, Y. H. Ultra-Transparent, Flexible Single-Walled Carbon Nanotube Non-Volatile Memory Device with an Oxygen-Decorated Graphene Electrode. *Adv. Mater.* **2011**, *23*, 1889−1893.
(35) Su, C.-Y.; Xu, Y.; Zhang, W.; Zhao, J.; Tang, X.; Tsai, C.-H.; Li, L.-J. Electrical and Spectroscopic Characterizations of Ultra-Large Reduced Graphene Oxide Monolayers. *Chem. Mater.* **2009**, *21*, 5674−5680.
(36) Yun, J. M.; Yeo, J. S.; Kim, J.; Jeong, H. G.; Kim, D. Y.; Noh, Y. J.; Kim, S. S.; Ku, B. C.; Na, S. I. Solution-Processable Reduced Graphene Oxide as a Novel Alternative to Pedot:Pss Hole Transport Layers for Highly Efficient and Stable Polymer Solar Cells. *Adv. Mater.* **2011**, *23*, 4923−4928.
(37) Dreyer, D. R.; Park, S.; Bielawski, C. W.; Ruoff, R. S. The Chemistry of Graphene Oxide. *Chem. Soc. Rev.* **2010**, *39*, 228−240.
(38) Moon, I. K.; Lee, J.; Ruoff, R. S.; Lee, H. Reduced Graphene Oxide by Chemical Graphitization. *Nat. Commun.* **2010**, *1*, 73.
(39) Jung, G. H.; Hong, K.; Dong, W. J.; Kim, S.; Lee, J.-L. Bcp/Ag/Moo3 Transparent Cathodes for Organic Photovoltaics. *Adv. Energy Mater.* **2011**, *1*, 1023−1028.
(40) Spoerke, E. D.; Lloyd, M. T.; McCready, E. M.; Olson, D. C.; Lee, Y.-J.; Hsu, J. W. P. Improved Performance of Poly(3-Hexylthiophene)/Zinc Oxide Hybrid Photovoltaics Modified with Interfacial Nanocrystalline Cadmium Sulfide. *Appl. Phys. Lett.* **2009**, *95*, 213506.
(41) Park, S. Y.; Kim, B. J.; Kim, K.; Kang, M. S.; Lim, K. H.; Lee, T. I.; Myoung, J. M.; Baik, H. K.; Cho, J. H.; Kim, Y. S. Low-Temperature, Solution-Processed and Alkali Metal Doped Zno for High-Performance Thin-Film Transistors. *Adv. Mater.* **2012**, *24*, 834−838.